International Journal of Scientific Research in Science and Technology
Available online at : www.ijsrst.com
Print ISSN: 2395-6011 | Online ISSN: 2395-602X
doi : https://doi.org/10.32628/IJSRST251246

On the Time to Stationarity of Peer-Driven Adoption and Event-Driven Abandonment of Digital Asset Trends on Social Networks

Agbedo E. I.*, Osanakpa R. O., Salami M. O, Kayoh C. O., Ugbene I. J
*Department of Mathematics, Federal University of Petroleum Resources, Effurun, Nigeria

ARTICLEINFO

Article History:

Accepted : 01 July 2025
Published: 15 July 2025

Publication Issue :
Volume 12, Issue 4
July-August-2025

Page Number :
314-338

ABSTRACT

This study explores the intricate dynamics of digital asset engagement, employing a Markov chain model to examine peer-influenced adoption (θ) and event-triggered abandonment (γ) across diverse network structures. The study gives hindsight into mixing time (time to stationarity) analysis, which represents the duration required to achieve a stationary distribution, and investigates its upper bound along with a revised linear programming proof. Simulations reveal the significant impact of network architecture on the spread of adoption and abandonment behaviors over time. Random networks typically demonstrate faster mixing, facilitating rapid information dissemination and market stabilization. In contrast, structured networks like small-world and scale-free exhibit more complex and often slower mixing patterns, showing distinct vulnerabilities or resilience based on the prevailing dynamic. Phase diagrams outline areas of sustainable adoption, critical decline, and swift abandonment, showcasing the long-term viability of various digital asset categories (such as Bitcoin-like, Meme coin-like, and NFT-like) within these network landscapes. The research underscores the crucial influence of network structure on market efficiency, information flow, and the enduring sustainability of digital assets. Additionally, this study aims to provide practical insights for Web3 project teams striving to cultivate sustainable asset ecosystems.

Keywords: Peer-influenced adoption, Event-triggered Abandonment, mixing time, stationary distribution, digital asset, network structures, information dissemination, market stabilization.

I. INTRODUCTION

The ever-growing landscape of digital assets and Web3 technologies is introducing a rather positive skewed transformation in economic and social paradigms (Sergio and Wedemeier, 2025). From cryptocurrencies such as Bitcoin to non-fungible tokens (NFTs) and decentralized finance (DeFi) protocols, these innovations are likely changing the primary methods by which value is created,

exchanged, and governed (ElBahrawy et al., 2017; Saiedi et al., 2021). Considerably, a very crucial factor in their long-term sustainability and impact is understanding the dynamics of user participation, specifically how large numbers of people begin to use them within their communities, and the reason why they cease using them, which could be due to external events or the actions of their peers (Angorani, 2024). Unlike traditional market systems, this digital asset world is known to be interconnected in complex ways, and the identities of several participants are often not publicly known (Kimmerl, 2020). Therefore, it is necessary to consider the network itself as the most important element to truly understand why some succeed and others fail. This is what we intend to study in detail. We want to create a model to observe how people behave within different types of networks. Our goal is to discover how the structure of the network (Li et al., 2018), its time to reach a stable distribution (mixing time also the time to stationarity) (Gao and Greenhill, 2020; Ramkumar and Soleimanifar, 2024), the probability at which people adopt these assets, and the probability at which they abandon them interact with each other (Kimmel et al., 2024; Kong, 2024; Fang et al., 2012). Ultimately, this will provide a better understanding that will contribute to the sustained growth and long-term usefulness of these new digital financial instruments.

The examination of intricate systems, especially using the methods of network science, has provided significant understanding in various areas, from how social behaviors spread to how diseases propagate. Within this broad area, how things are adopted and then abandoned has been studied a lot (Ebizie et al., 2022; Shahzad et al., 2024), often using tools like Markov chains and computer-based models. Early work on how a product becomes more valuable as more people use it showed this is very important for new digital platforms to grow at the start (Pesch et al., 2021; Kremer et al., 2013). At the same time, research on how information spreads across different network types including, random, small-world, and scale-free networks, has shown how the way connections are organized affects how fast and how far things spread. These studies have found that networks where many people are connected in small groups and where it's easy to get from one person to another quickly (small-world networks) can help things spread globally very fast. Also, scale-free networks, which have a few very connected individuals linking many less connected ones, are good at spreading things because of these central hubs (Cipriani and Salvi, 2021; Blumberg et al., 2024).

More recently, these ideas have been used more and more in the new field of digital assets and blockchain. Researchers have started to see the adoption of cryptocurrencies as similar to how social behaviors spread, looking at how friends and the benefits of more users encourage people to join (Boralkar et al., 2024; Nuwan et al., 2025). At the same time, the idea of people stopping their use, which wasn't focused on in early growth models, has become more important, especially because digital asset markets change quickly and are affected by events. Studies have begun to think about how sudden price drops, security problems, or changes in rules can be key "abandonment events" that can greatly change what users do (John et al., 2024; Hafid et al., 2024). While current studies give basic models for how networks work and how adoption and abandonment happen in different situations, there's still a big need to fully understand how peer influence, regular adoption patterns, sudden abandonment events, and the specific structures of different network types interact in the unique and fast-changing world of digital assets (Allassak et al., 2024; Rodpangtiam et al., 2024; Kajol et al., 2025). Moreover, the idea of people being hesitant to start using something again after they've stopped, which is important in real life, hasn't been looked at much in current network models of digital asset use.

Therefore, drawing from prior research in network science (Emunefe and Ugbene, 2024; Osanakpa and Ugbene, 2025; Kayoh and Ugbene, 2023; Ugbene and

Utoyo, 2024b; Ugbene and Agwemuria, 2024; Ugbene and Utoyo, 2024a; Ugbene and Ajuremisan, 2025) and combinatorial algebra (Ugbene and Makanjuola, 2012; Ugbene et al., 2013; Ugbene and Mbah, 2015; Ugbene et al., 2019, 2022), this paper sets out to investigate the developing patterns of how digital assets are adopted and then abandoned within different kinds of network frameworks. The study will use Markov chain theory as a tool to assess how stable user involvement is. It will also examine how interactions with other users and events happening outside the network influence the time it takes for the system to settle into a balanced state, as well as how significant these assets will remain over time. Furthermore, this research also aim to provide useful advice for teams working on Web3 projects about how to encourage lasting growth and ensure their systems continue to function effectively within these decentralized environments.

II. METHODS AND MATERIAL

We propose a discrete-time Markov chain model to analyze the adoption and abandonment of digital assets. This model draws inspiration from epidemiological compartmental processes (Ahn and Hassibi, 2014) and social contagion theory but is tailored to reflect the unique characteristics of digital asset propagation. The model considers a connected, undirected network G with n agents (nodes), where each agent's peers are represented by the set $\mathcal{N}_i$. The network's structure is described by the adjacency matrix $\mathcal{A}$.

Agents can be in one of two states: non-adoption (abandonment), denoted as "N_a or $\bar{0}$", or adoption, denoted as "A_d or $\bar{1}$". The system's state at time τ is represented by

$$\eta(\tau) = (\eta_1(\tau), \dots, \eta_n(\tau)) \in \{N_a, A_d\}^n$$

Here, $\eta_i(\tau) = A_d$ indicates that agent i has adopted the digital asset at time τ, and $\eta_i(\tau) = N_a$ indicates abandonment or non-adoption. The model assumes that the probability of (re)adoption for each agent is independent of others, given the current system state. That is, for any two configurations $W, Z \in \{N_a, A_d\}^n$,

$$\mathbb{P}[\eta(\tau+1) = Z|\eta(\tau) = W] = \prod_{i=1}^{n} \mathbb{P}\left[\eta_i(\tau+1) = Z_i|\eta(\tau) = W\right] \quad (1)$$

Also, an agent remains in the non-adoption state if none of its peers are adopters. Adoption may occur due to influence from any adopting neighbor, with each influence happening independently with probability θ. Adopters may abandon the asset with probability γ, unless immediately re-influenced by peers.

However, static probability assumptions often fail to capture the dynamic behavioral patterns observed in real-world digital asset ecosystems. Both abandonment and adoption probabilities exhibit temporal variations driven by external stimuli, sentiment evolution, and market dynamics. Adoption rates may decay as initial hype diminishes (e.g., for NFTs) or grow due to positive feedback and network effects (e.g., for Bitcoin). The abandonment probability γ may follow a uniform distribution and increase due to asset depreciation, loss of trust, or negative external events. Alternatively, abandonment might spike due to abrupt external events, such as scandals. This behavior can be modeled using a sigmoid function, such that

$$\gamma \to \gamma(t) = \gamma_{\max} \cdot \frac{1}{1+e^{-k_\gamma(t-t_0)}} \quad (2)$$

Here, the peak likelihood of abandonment is represented by $\gamma_{\max}$, while k_γ denotes the rate of change in the transition, and t_0 signifies the moment when a notable event or shock first occurs. To represent increased participation, usage, or growing social interest (such as in the case of meme stocks), we employed an adoption likelihood (θ) that also adheres to a uniform distribution. However, adoption patterns may also exhibit cyclical trends, particularly during anticipated events like cryptocurrency halving cycles. A cosine-based model effectively captures this periodic nature

$$\theta \to \theta(t) = \theta_0 + \Delta_\theta \left|\cos\left(\frac{2\pi t}{T}\right)\right| \quad (3)$$

where, the baseline adoption influence is represented by α_0, while $\Delta_\alpha \in [0.01,0.05]$, denotes the magnitude of fluctuation. T signifies the cycle's duration, which is 365 for yearly cycles. This formulation would result in a periodic Markov chain without a convergence time, reflecting the actual behavior of digital asset value over time. However, when considering the time to stationarity, we employ an aperiodic and irreducible Markov chain model, which can be concisely described as follows:

$$\mathbb{P}[\eta_i(\tau+1) = Z_i | \eta(\tau) = W] = \begin{cases} (1-\theta)^{k_i} & \text{if}(W_i, Z_i) = (N_a, N_a), |\mathcal{N}_i \cap \mathbb{A}(W)| = k_i \\ 1-(1-\theta)^{k_i} & \text{if}(W_i, Z_i) = (N_a, A_d), |\mathcal{N}_i \cap \mathbb{A}(W)| = k_i \\ \gamma(1-\theta)^{k_i} & \text{if}(W_i, Z_i) = (A_d, N_a), |\mathcal{N}_i \cap \mathbb{A}(W)| = k_i \\ 1-\gamma(1-\theta)^{k_i} & \text{if}(W_i, Z_i) = (A_d, A_d), |\mathcal{N}_i \cap \mathbb{A}(W)| = k_i \end{cases} \quad (4)$$

where the set of current adopters is denoted as $\mathbb{A}(W)$, which includes all nodes j where $W_j = A_d$. The transition matrix T of this Markov Chain is defined by the probability of moving from state W to state Z in one time step, represented as $T_{W,Z} = \mathbb{P}[\eta(\tau+1) = Z|\eta(\tau) = W]$. Assuming time-homogeneity, this can be simplified to $T_{W,Z} = \mathbb{P}[Z|W]$. In this Markov chain model of peer-influenced digital asset adoption and abandonment, there exists an absorbing state where all network nodes are inactive, having abandoned the digital asset. Once this all-inactive state is reached, the network remains in this state indefinitely, as the model does not account for external factors or spontaneous adoptions that are independent of peer influence. As time advances, the probability distribution across the states $\{N_a, A_d\}^n$ tends towards the completely inactive state. This implies that, given sufficient time, abandonment will ultimately prevail. However, this theoretical outcome may not always be practical in real-world scenarios. The reason is that the mixing time of the Markov chain, which represents the duration required to approach the absorbing state, can be exceedingly long, particularly in large-scale networks. As a result, analyzing the system's dynamic behavior becomes computationally intensive as the network size increases. Let $A(\tau)$ represent the group of active (adopting) nodes at a given time τ. Define

$$q_j(\tau) = \mathbb{P}[j \in A(\tau)]$$

as the probability that node j is actively using the digital asset at time τ. Then, the evolution of $q_j(\tau)$ can be expressed as

$$q_j(\tau+1) = \mathbb{P}[j \in A(\tau+1) \mid j \in A(\tau)] \cdot q_j(\tau) + \mathbb{P}[j \in A(\tau+1) \mid j \notin A(\tau)] \cdot (1-q_j(\tau)) \quad (5)$$

Using the transition probabilities from the node-level adoption model in (4), we rewrite this as

$$q_j(\tau+1) \& = 1-\gamma(1-\theta)^{k_j(\tau)} q_j(\tau) + (1-(1-\theta)^{k_j(\tau)})(1-q_j(\tau)) \quad (6)$$

where

$$k_j(\tau) = |\mathcal{N}_i \cap A(\tau)|$$

is the number of active neighbors of node j at time τ. To simplify analysis, we approximate the discrete product term $(1-\theta)^{k_j(\tau)}$ using the expectation assuming independence of neighbors' states:

$$\prod_{i \in \mathcal{N}_i} (1-\theta \mathbf{1}_{A(\tau)}(i)) \approx \prod_{i \in \mathcal{N}_i} (1-\theta q_i(\tau)).$$

Thus, the approximated adoption probability dynamics become

$$Q_j(\tau+1) = 1-\gamma\left(\prod_{i \in \mathcal{N}_i} (1-\theta Q_i(\tau))\right) Q_j(\tau) + (1 - \prod_{i \in \mathcal{N}_i} (1-\theta Q_i(\tau)))(1 - Q_j(\tau)) \quad (7)$$

where $Q_j(\tau)$ denotes the approximated probability of node j adopting the digital asset at time τ, also note that $Q_j(\tau)$ is the approximate probability of the markov chain model, while $q_j(\tau)$ is exact. This approximated model operates over the continuous space $[N_a, A_d]^n$, which is computationally more tractable than the original discrete state space of size 2^n. Following the approach of previous studies on dynamics of network systems (Chakrabarti et al., 2008; Ahn and Hassibi, 2014), define the nonlinear map $\Psi: [N_a, A_d]^n \to [N_a, A_d]^n$ with components

$$\Psi_j(x) = (1-\gamma)x_j + (1-(1-\gamma)x_j)\left(1-\prod_{i\in\mathcal{N}_i}(1-\theta x_i)\right) \quad (8)$$

It is straightforward to verify that the update rule in (7) satisfies

$$Q_j(\tau+1) = \Psi_j(Q_1(\tau), Q_2(\tau), \dots, Q_n(\tau))$$

The map Ψ captures the combined effects of abandonment (parameter γ) and peer-driven adoption (parameter θ) over the network, providing a nonlinear dynamical system perspective on digital asset adoption dynamics.

2.1 Time to Stationarity and Partial Order on Probability Vectors

The *time to stationarity or stationary distribution convergence time (also mixing time)* of the Markov chain $(\eta(\tau))_{\tau\geq 0}$ on the state space $\{N_a, A_d\}^n$ is a key concept in understanding how quickly the chain converges to its stationary distribution. It is defined as follows (see also (Ruhi and Hassibi, 2015; Ahn and Hassibi,2014)):

$$\tau_{\text{mix}}(\varepsilon) = \min\{\tau : \sup_{\omega} \| \omega\mathcal{X}^{\tau} - \Omega\|_{\mathcal{TV}} \leq \varepsilon\} \quad (9)$$

where ω is an arbitrary initial probability distribution over the states, $\mathcal{X}$ is the transition matrix of the Markov chain, Ω is the unique stationary distribution supported on the absorbing non-adoption state, and $\|\cdot\|_{\mathcal{TV}}$ denotes the total variation distance. To analyze the mixing time more effectively, we introduce a *partial order* $\geq_{\mathcal{P}}$ on the set of probability distributions over $\{N_a, A_d\}^n$. This partial order allows us to identify a maximal initial distribution ω that attains the supremum in (9).

Definition 2.1 (Partial order $\geq_{\mathcal{P}}$ on probability distributions). For two probability vectors $\omega, \omega' \in \mathbb{R}^{2^n}$ defined on $\{N_a, A_d\}^n$, we say

$$\omega \geq_{\mathcal{P}} \omega' \text{ if and only if } \sum_{W\leq Y}\mu_X \geq \sum_{W\leq Y}\omega'_W, \quad \forall\ Y \in \{N_a, A_d\}^n \quad (10)$$

where $W \leq Y$ means $W_i \leq Y_i$ for all $i = 1, \dots, n$. Here, ω_W denotes the probability assigned to state W by ω. Intuitively, the sum $\sum_{W\leq Y}\omega_W$ corresponds to the probability that all nodes in the complement of the infected set $\mathcal{X}(Y)$, denoted $\mathcal{X}(Y)^c$, are healthy. Hence, $\omega \geq_{\mathcal{P}} \omega'$ means the distribution ω assigns higher probabilities to configurations with more non-adoption nodes compared to ω', for any given subset of nodes. Let $e_W \in \mathbb{R}^{2^n}$ denote the unit vector with a 1 in the coordinate corresponding to state W and zeros elsewhere. Denote the non adoption and adoption states by $\overline{N_a}, \overline{A_d} \in \{N_a, A_d\}^n$, respectively. Clearly, $e_{\overline{N_a}}$ is the maximal element and $e_{\overline{A_d}}$ the minimal element under $\geq_{\mathcal{P}}$. Since $\overline{N_a}$ is absorbing in the Markov chain, $e_{\overline{N_a}}$ is the unique stationary distribution. The key property of $\geq_{\mathcal{P}}$ is that it makes the transition operator $\mathcal{X}$, *order-preserving*:

$$\omega \geq_{\mathcal{P}} \omega' \rightarrow \omega\mathcal{X} \geq_{\mathcal{P}} \omega'\mathcal{X} \quad (11)$$

To establish this property, we introduce the following lemma.

Lemma 2.1. Let $\mathcal{L} \in \mathbb{R}^{2^n\times 2^n}$ be the matrix defined by

$$\mathcal{L}_{W,Z} = \begin{cases} 1 & \text{if } W \leq Z, \\ 0 & \text{otherwise.} \end{cases} \quad (12)$$

Then, the matrix $\mathcal{L}^{-1}\mathcal{X}\mathcal{L}$ has non-negative entries.

Proof

First, define the matrix $\mathcal{L}' \in \mathbb{R}^{2^n\times 2^n}$ by

$$\mathcal{L}'_{W,Z} = \begin{cases} (-1)^{|\mathcal{X}(Z-W)|} & \text{if } W \leq Z, \\ 0 & \text{otherwise,} \end{cases} \quad (13)$$

Where $\mathcal{X}(Z-W)$ is the set of nodes infected in Z but not in W. We claim that $\mathcal{L}' = \mathcal{L}^{-1}$. Indeed, for $W \not\leq Z$, either $W \not\leq Z$ or $Y \not\leq Z$ for all Y, so $(\mathcal{L}\mathcal{L}')_{W,Z} = 0$. For $W \leq Z$, we compute

$$(\mathcal{L}\mathcal{L}')_{W,Z} = \sum_{Y}\mathcal{L}\ \mathcal{L}'_{Y,Z} = \sum_{W\leq Y\leq Z}(-1)^{|\mathcal{X}(Z-Y)|} = (1-1)^{|\mathcal{X}(Z-W)|} = \begin{cases} 1 & \text{if} |\mathcal{X}(Z-W)| = 0, \\ 0 & \text{otherwise,} \end{cases} \quad (14)$$

which is the identity matrix. Hence, $\mathcal{L}' = \mathcal{L}^{-1}$. Next, consider the matrix product

$$(\mathcal{L}^{-1}\mathcal{X}\mathcal{L})_{W,Y} = \sum_{Z\le Y}(\mathcal{L}^{-1}\mathcal{X})_{W,Z} = \sum_{Z\le Y}\sum_{V}\mathcal{L}^{-1}_{W,V}\,\mathcal{X}_{V,Z}$$
$$= \sum_{Z\le Y}\sum_{V\ge W}(-1)^{|\mathcal{L}(V-W)|}\mathcal{L}_{V,Z}$$
$$= \sum_{V\ge W}(-1)^{|\mathcal{X}(V-W)|}\prod_{i\in\mathcal{L}(Y)^c}\mathbb{P}[\eta_i(\tau+1) = N_a \mid \eta(\tau) = W]$$
$$= \sum_{V\ge W}(-1)^{|\mathcal{X}(V-W)|}\gamma^{|\mathcal{L}(V)\cap\mathcal{X}(Y)^c|}(1-\theta)^{\sum_{i\in\mathcal{X}(Y)^c}|\mathcal{N}_i\cap\mathcal{X}(V)|}$$
$$= \sum_{V\ge W}(-1)^{|\mathcal{X}(V-W)|}\gamma^{|\mathcal{X}(V)\cap\mathcal{X}(Y)^c|}(1-\theta)^{\sum_{i\in\mathcal{X}(V)}|\mathcal{N}_i\cap\mathcal{X}(Y)^c|} \quad (15)$$

By algebraic manipulation,

$$\gamma^{-|\mathcal{X}(W)\cap\mathcal{X}(Y)^c|}(1-\theta)^{-\sum_{i\in\mathcal{X}(W)}|\mathcal{N}_i\cap\mathcal{X}(Y)^c|}(\mathcal{L}^{-1}\mathcal{X}\mathcal{L})_{W,Y}$$
$$= \sum_{V\ge W}(-1)^{|\mathcal{X}(V-W)|}\gamma^{|\mathcal{X}(V-W)\cap\mathcal{X}(Y)^c|}(1-\theta)^{\sum_{i\in\mathcal{X}(V-W)}|\mathcal{N}_i\cap\mathcal{X}(Y)^c|}$$
$$= \prod_{i\in\mathcal{X}(W)^c}\left(1-(1-\theta)^{|\mathcal{N}_i\cap\mathcal{X}(Y)^c|}\gamma^{\mathbf{1}_{i\in\mathcal{X}(W)^c}}\right) \quad (16)$$

Define the complement operator $\neg W = \overline{1} - W$. Using this notation, we rewrite the entries of $\mathcal{L}^{-1}\mathcal{X}\mathcal{L}$ as

$$(\mathcal{L}^{-1}\mathcal{X}\mathcal{L})_{W,Y} = \mathbb{P}[\eta(\tau+1) = \neg W \mid \eta(t) = \neg Y] \ge 0 \quad (17)$$

Since all entries of $\mathcal{L}^{-1}\mathcal{X}\mathcal{L}$ are non-negative, this establishes the order-preserving property of $\mathcal{X}$ under $\succeq_{\mathcal{P}}$. Thus, the partial order $\succeq_{\mathcal{P}}$ allows us to characterize the monotonicity of the Markov chain dynamics and to bound the stationary distribution convergence time by examining extremal initial distributions. This is crucial in the analysis of peer-driven digital asset adoption and abandonment where the state space size grows exponentially with the number of nodes.

Lemma 2.2. If $\omega \succeq_{\mathcal{P}} \omega'$, then $\omega\mathcal{X} \succeq_{\mathcal{P}} \omega'\mathcal{X}$.

Proof

By the definition of $\omega \succeq_{\mathcal{P}} \omega'$,

$$((\omega-\omega')\mathcal{L})_Z = \sum_W(\omega-\omega')_W\mathcal{L}_{W,Z}$$
$$= \sum_{W\le Z}(\omega-\omega')_W \ge 0 \quad (18)$$

Also, $((\omega-\omega')\mathcal{L})_{\overline{1}} = 0$ if $Z = \overline{1} = (1,1,\dots,1)$ since both ω and ω' are probability vectors (i.e., $1-$norm equals 1). Define a row vector $r \in \mathcal{L}^{\{0,1\}^n}$ such that $r_Z = ((\omega-\omega')\mathcal{L})_Z$. By \eqref{eq:23}, we know $r_Z \ge 0 \ \forall\ Z \in \{0,1\}^n$, and $r_{\overline{1}} = 0$. Therefore, $\omega-\omega' = r\,\mathcal{L}^{-1}$. That is, $\omega-\omega'$ is a conical combination of the rows of $\mathcal{L}^{-1}$ except the $\overline{1}$-th row. Thus, $\omega \succeq_{\mathcal{P}} \omega'$ if and only if $(\omega-\omega')\mathcal{L}$ is a vector with non-negative entries.

To show $\omega\mathcal{X} \succeq_{\mathcal{P}} \omega'\mathcal{X}$, we check if $(\omega-\omega')\mathcal{X}\mathcal{L}$ is non-negative. Since $\omega-\omega' = r\mathcal{L}^{-1}$ and $r \ge 0$, we have:

$$(\omega-\omega')\mathcal{X}\mathcal{L} = r\mathcal{L}^{-1}\mathcal{X}\mathcal{L},$$

which is non-negative because $\mathcal{L}^{-1}\mathcal{X}\mathcal{L}$ has all non-negative entries by Lemma (2.1). By Lemma (2.2), for any probability vector ω such that $\omega \succeq_{\mathcal{P}} g_{\overline{1}}$, it follows:

$$\sum_{W\le\overline{0}}(\omega\mathcal{X}^\tau)_X - (\omega\mathcal{X}^\tau)_{\overline{0}} \ge (g_{\overline{1}}\mathcal{X}^\tau)_{\overline{0}} - \sum_{W\le\overline{0}}(g_{\overline{1}}\mathcal{X}^\tau)_W.$$

Recall the definition of stationary distribution convergence time:

$$\|\omega\mathcal{X}^\tau - \Omega\|_{\mathcal{TV}} \& = \|\omega\mathcal{X}^\tau - g_{\overline{0}}\|_{\mathcal{TV}} = 1 - (\omega\mathcal{X}^\tau)_{\overline{0}}$$
$$\le 1 - (g_{\overline{1}}\mathcal{X}^\tau)_{\overline{0}}$$
$$= 1 - g_{\overline{1}}\mathcal{X}^\tau g_{\overline{0}}^T \quad (19)$$

Hence, the stationary distribution convergence time satisfies:

$$\tau_{\text{mix}}(\varepsilon) = \min\{\tau: \sup_\omega \|\omega\mathcal{X}^\tau - \Omega\|_{\mathcal{TV}} \le \varepsilon\}$$
$$= \min\{\tau: 1 - g_{\overline{1}}\mathcal{X}^\tau g_{\overline{0}}^T \le \varepsilon\}$$
$$= \min\{\tau: g_{\overline{1}}\mathcal{X}^\tau g_{\overline{0}}^T \ge 1-\varepsilon\} \quad (20)$$

2.2 Upper Bound on the Stationary distribution Convergence time

Here, we show that the digital asset adoption map $\widetilde{\Psi}(\cdot)$, defined as in equation (8), provides an upper bound on the stationary distribution convergence time of the Markov chain. This leads to a practical bound. We aim to find a lower bound for $g_{\overline{1}}\mathcal{X}^\tau g_{\overline{0}}^T$ to obtain an upper bound on $\tau_{\text{mix}}(\varepsilon)$. Define a 2^n-dimensional column vector $f(e)$ for $e = (e_1,\dots,e_n)^T \in [0,1]^n$ by:

$$f(e)_W = \prod_{i\in\mathcal{X}(W)}(1-e_i)$$

We seek $e' \in \mathbb{R}^n$ such that $\mathcal{X}f(e) \geq f(e')$.

Lemma 2.3. $\mathcal{X}f(e) \geq f(\Psi(e))$ for all $e \in [0,1]^n$.

Proof. Evaluate each entry of $\mathcal{X}f(e)$:

$$(\mathcal{X}f(e))_W = \sum_{Z\in\{0,1\}^n} \mathcal{X}_{W,Z} f(e)_Z = \sum_{Z\in\{0,1\}^n} \left(\prod_{i\in\mathcal{X}(Z)} (1-e_i)\mathbb{P}[Z_i = 1|W]\right)\left(\prod_{i\notin\mathcal{X}(Z)} \mathbb{P}[Z_i = 0|W]\right) = \prod_{i=1}^{n}((1-e_i)\mathbb{P}[Z_i = 1|W] + \mathbb{P}[Z_i = 0|W]) \quad (21)$$

Assuming disjoint support sets $\mathcal{X}(W) \cap \mathcal{X}(Y) = \emptyset$, we observe:

$$\mathbb{P}[Z_k = 0|W+Y] = \mathbb{P}[Z_k = 0|W]\mathbb{P}[Z_k = 0|Y] \quad (22)$$

Let $q_{k,W} = \mathbb{P}[Z_k = 0|W]$. Then:

$$(\mathcal{X}f(e))_{W+Y} = \prod_{i=1}^{n}\big((1-e_i)(1-q_{i,W+Y}) + q_{i,W+Y}\big) = \prod_{i=1}^{n}\big((1-e_i)(1-q_{i,W}q_{i,Y}) + q_{i,W}q_{i,Y}\big) \geq \prod_{i=1}^{n}\big((1-e_i)(1-q_{i,W}) + q_{i,W}\big)\big((1-e_i)(1-q_{i,Y}) + q_{i,Y}\big) = (\mathcal{X}f(e))_W(\mathcal{X}f(e))_Y \quad (23)$$

Inequality (23) follows from the identity:

$$(z(1-xy)+xy) - (z(1-x)+x)(z(1-y)+y) = z(1-z)(1-x)(1-y) \geq 0, \quad \text{for } x,y,z \in [0,1]$$

Define $\hat{\imath} \in \{0,1\}^n$ as the state with only node i as an adopter. Then from (23):

$$(\mathcal{X}f(e))_W \geq \prod_{i\in\mathcal{X}(W)} (\mathcal{X}f(e))_{\hat{\imath}} = \prod_{i\in\mathcal{X}(W)}\prod_{j=1}^{n}\big((1-e_j)\mathbb{P}[Z_j = 1|\hat{\imath}] + \mathbb{P}[Z_j = 0|\hat{\imath}]\big) = \prod_{i\in\mathcal{X}(W)}((1-e_i)(1-\gamma)+\gamma)\prod_{j\sim i}\big((1-e_j)\theta + 1 - \theta\big) = \prod_{i\in\mathcal{X}(W)}(1-(1-\gamma)e_i)\prod_{j\sim i}(1-\theta e_j) = \prod_{i\in\mathcal{X}(W)}(1-\widetilde{\Psi}_i(e)) = f(\widetilde{\Psi}(e))_W \quad (24)$$

Since $\mathcal{X}f(e) \geq f(\widetilde{\Psi}(e))$ and $\mathcal{X}$ is non-negative:

$$\mathcal{X}^\tau g_0^T = \mathcal{X}f(\overline{1}_n) \geq f(\widetilde{\Psi}^\tau(\overline{1}_n)) \quad (25)$$

Let us define the system matrix of the linearized adoption dynamics as $\mathcal{M} = (1-\gamma)A_{d_n} + \theta\mathcal{A}$, which corresponds to the Jacobian of the function $\Psi(\cdot)$ evaluated at the null state (i.e., no adoption). Consider the nonlinear update rule governing the evolution of adoption states:

$$\widetilde{\Psi}_\tau(y) = (1-\gamma)y_i + (1-\gamma)y_i\left(1 - \prod_{j\sim i}(1-\theta y_j)\right) \leq (1-\gamma)y_i + \left(1 - \prod_{j\sim i}(1-\theta y_j)\right) \leq (1-\gamma)y_i + \theta\sum_{j\in\mathcal{N}_i} y_j = (\mathcal{M}y)_i \quad (26)$$

The derivation above provides an upper bound on the nonlinear influence function $\widetilde{\Psi}$ using the linear transformation $\mathcal{M}y$, such that $\widetilde{\Psi}(y) \leq \mathcal{M}y$. This bound enables a useful result on the convergence behavior of the adoption dynamics under the assumption that the matrix $\mathcal{M}$ is stable, meaning its spectral radius is strictly less than 1.

Theorem 2.1. If $\|\mathcal{M}\| < 1$, then the stationary distribution convergence time satisfies $\tau_{\text{mix}}(\xi) = O(\log n)$.

Proof

Assume $\tau \leq \tau_{\text{mix}}(\xi)$. Then, we analyze the decay of the adoption signal as follows:

$$1-\xi \geq g_1^{\top}\mathcal{X}_{\tau}^{\top}g_0 \geq g_1^{\top}f(\widetilde{\Psi}^{\tau}(\mathbf{1}_n))$$
$$= \prod_{j=1}^{n}(1-\widetilde{\Psi}_j^{\tau}(\mathbf{1}_n)) \geq 1-\sum_{j=1}^{n}\widetilde{\Psi}_j^{\tau}(\mathbf{1}_n)$$
$$\geq 1-n\sqrt{\frac{1}{n}\sum_{j=1}^{n}(\widetilde{\Psi}_j^{\tau}(\mathbf{1}_n))^2} = 1-\sqrt{n}\|\widetilde{\Psi}^{\tau}(\mathbf{1}_n)\|$$
$$\geq 1-\sqrt{n}\|\mathcal{M}^{\tau}\mathbf{1}_n\| \geq 1-\sqrt{n}\|\mathcal{M}\|^{\tau}\|\mathbf{1}_n\|$$
$$= 1-n\|\mathcal{M}\|^{\tau} \qquad (27)$$

To ensure the deviation is less than ξ , it suffices that:

$$n\|\mathcal{M}\|^{\tau} \leq \xi \;\Rightarrow\; \tau \geq \frac{\log(n/\xi)}{-\log\|\mathcal{M}\|}$$

Hence, the upper bound on the stationary distribution convergence time is given by:

$$\tau_{\text{mix}}(\xi) \leq \frac{\log(n/\xi)}{-\log\|\mathcal{M}\|}$$

which grows logarithmically with the size of the network, i.e., $\tau_{\text{mix}}(\xi) = O(\log n)$.

In scenarios where $\|\mathcal{M}\| > 1$, the iterative sequence $\widetilde{\Psi}^{\tau}(1_n)$ converges to a nontrivial fixed point y^* of the adoption map $\widetilde{\Psi}$, with $y^* \gg 0$, as characterized in (Ann and Hassibi, 2014). This outcome reflects sustained participation across the network, contrasting the baseline Markov chain model, which ultimately stabilizes at the "no-adoption" absorbing state. The reason for this apparent discrepancy is that the i −th component of $\widetilde{\Psi}^{\tau}(1_n)$ upper bounds the probability that node i is still active in digital asset adoption, starting from a configuration where only node i participates initially. More formally, we have:

$$\widetilde{\Psi}_i^{\tau}(1_n) \geq 1-g_i^{T}\mathcal{X}^{\tau}g_0^{T}$$
$$= 1-\mathbb{P}[\eta(\tau)=\bar{0} \mid \eta(0)=\hat{\imath}]$$
$$= \mathbb{P}[\eta(\tau)\neq\bar{0} \mid \eta(0)=\hat{\imath}] \qquad (28)$$

This inequality implies that if the digital adoption map $\widetilde{\Psi}$ has a globally stable equilibrium at the origin, then the corresponding Markov process (modeling node-level adoption states) will exhibit rapid convergence to the no-adoption state, i.e., fast mixing. Conversely, when the origin is unstable in the deterministic approximation $\widetilde{\Psi}$, the system might sustain long-term adoption, but then this does not guarantee or imply any specific mixing behavior for the underlying stochastic model.

2.3 Reformulated Proof via Linear Programming

Building on the work of Ahn and Hassibi (2014) regarding mixing times, our analysis indicates that a specific nonlinear function, denoted as $\widetilde{\Psi}(\cdot)$, sets a limit on how likely it is for any given participant in the network-based adoption process to adopt the digital asset. However, to show that the average time it takes for adoption to spread significantly is roughly proportional to the logarithm of the network size $O(\log n)$, it is enough to prove a less strict condition. This condition is that a simplified, linear version of the system can act as a reliable upper limit. Remarkably, it's probable that this can be shown using a simpler argument based on linear programming.

Let $\omega(\tau)$ be a mathematical representation (a row vector) of the probabilities of all possible adoption scenario within the networks at a specific times τ. Here, $\{0,1\}^n$ represents all the ways n participants can either have adopted (1) or not adopted (0) the digital asset. For any individual participant i in the network, the basic probability of them having adopted the asset at time τ can be written, apparently as:

$$p_i(\tau) = \sum_{W\in\{0,1\}^n : W_i=1} \omega_W(\tau)$$

where $W_i = 1$ signifies that node i has adopted the digital asset in state W. Define $p_0(\tau) = 1 - \sum_W \omega_W(\tau)$, representing the mass associated with unobserved or external states. Now define the column vector of adoption probabilities and residual mass as:

$$p(\tau) = (p_0(\tau), p_1(\tau), \dots, p_n(\tau))^{\top}$$

We consider $p(\tau)$ as the adoption information we can see at a specific time τ, while $\omega(\tau)$ remains the complete, underlying condition of the system that we cannot directly observe. Our aim is to develop a way to estimate the limit for $p(\tau+1)$, which is what we expect to see at the next point in time, using only the information we currently have. To do this, let h_i be a basic vector that helps us focus on a specific part of the system's state. Let $\mathcal{X}$ be the transition matrix, which describes how the digital adoption process changes over time. We will also define a matrix $\mathcal{M}$ that helps us connect the full underlying state to the

observable information. This matrix $\mathcal{M}$ starts with a column of all ones (representing the initial state where no one has adopted, p_0), followed then by a systematic listing of every possible adoption statuses of each individual in the network across all 2^n possibilities. The detailed structure of $\mathcal{M}$ and how we find the upper limit can be mathematically expressed as:

$$p(\tau) = (p_0(\tau), p_1(\tau), \dots, p_n(\tau))^{\top}$$

We interpret $p(\tau)$ as observable adoption data at time τ, whereas the full state distribution $\omega(\tau)$ represents the latent state of the system. Our goal is to construct an upper bound for $p(\tau+1)$, the observable state at the next time step, based solely on current observations. To proceed, let $h_i \in \mathbb{R}^{n+1}$ denote the standard basis (unit) vector corresponding to the i-th coordinate. Let $\mathcal{X}$ represent the transition matrix of the digital adoption Markov process. Define a matrix $\mathcal{M} \in \mathbb{R}^{2^n \times (n+1)}$ that maps the full latent state to observable statistics. This matrix $\mathcal{M}$ contains a leading all-ones column (capturing p_0) followed by a binary truth table encoding the adoption status of each node in all 2^n configurations. The formal structure of $\mathcal{M}$ and the derivation of the upper bound can be represented as:

$$\mathcal{M}_{W,k} = \begin{cases} 1 & \text{if } k = 0, \\ W_k & \text{if } k \in \{1,2,\cdots,n\} \end{cases} \tag{29}$$

We aim to optimize $p_i(\tau+1)$ for a specific node i, based on the values of $p_1(\tau), \dots, p_n(\tau)$. This results in the following outcome.

Lemma2.4

$p_i(\tau+1) \le (1-\gamma)p_i(\tau) + \theta \sum_{j \in \mathcal{N}_i} p_j(\tau)$

Proof

For simplicity, we will omit the time index τ and only indicate the time index for $\tau+1$ in this proof from this point forward.

$$\max_{\omega\mathcal{M}=p^T,\omega\ge 0} p_i(\tau+1) = \max_{\omega\mathcal{M}=p^T,\omega\ge 0} \omega\,\mathcal{X}\mathcal{M}h_i$$
$$= \max_{\omega\ge 0}\min_{\varphi} \omega\,\mathcal{X}\mathcal{M}h_i - (\omega\mathcal{M} - p^T)\varphi$$
$$= \min_{\varphi}\max_{\omega\ge 0} \omega\,(\mathcal{X}\mathcal{M}h_i - \mathcal{M}\varphi) + p^T\varphi \tag{30}$$

$\max_{\omega\mathcal{M}=p^T,\omega\ge 0} \omega\,(\mathcal{X}\mathcal{M}h_i - \mathcal{M}\varphi) = +\infty$, if any entry of $(\mathcal{X}\mathcal{M}h_i - \mathcal{M}\varphi)$, is strictly positive. This implies that $\mathcal{X}\mathcal{M}h_i - \mathcal{M}\varphi \le 0$. Next, we evaluate $\mathcal{X}\mathcal{M}h_i$ and $\mathcal{M}\varphi$:

$$(\mathcal{X}\mathcal{M}h_i)_W = (\mathcal{X}\mathcal{M})_{W,i}$$
$$= \sum_{Z\in\{0,1\}^n} \mathcal{X}_{W,Z}\,\mathcal{M}_{Z,i} = \sum_{Z\in\{0,1\}^n} \mathcal{X}_{W,Z}\,Z_i$$
$$= \mathbb{P}[Z_i = 1|W]$$
$$= \begin{cases} 1-(1-\theta)^{k_i} & \text{if} W_i = 0, \\ 1-\gamma(1-\theta)^{k_i} & \text{if} W_i = 1 \end{cases} \tag{31}$$

The expression $\mathbb{P}[Z_i = 1|W]$ is derived from (4), where k_i represents the number of neighboring adopters of node i.

$$(\mathcal{M}\varphi)_W = \varphi_0 + \sum_{k=1}^{n} \mathcal{M}_{W,k}\,\varphi_k$$
$$= \varphi_0 + \sum_{k=1}^{n} \varphi_k W_k \tag{32}$$

We examine various W for (31), (32) and find that $\mathcal{X}\mathcal{M}h_i - \mathcal{M}\varphi \le 0$ to determine feasible φ:

$$\begin{cases} W = \overline{0}, & \varphi_0 \ge 0 \\ W = \hat{\imath}, & \varphi_0 + \varphi_i \ge 1-\gamma \\ W = \hat{\jmath}, j \in N_i, & \varphi_0 + \varphi_j \ge \theta \\ W = \hat{\jmath}, j \notin N_i, & \varphi_0 + \varphi_j \ge 0 \end{cases} \tag{33}$$

We assert that $\varphi^* = (\varphi_0^*, \varphi_1^*, \dots, \varphi_n^*)^T$ defined by $\lambda_0^* = 0, \varphi_i^* = 1-\gamma, \varphi_j^* = \theta$ for $j \in \mathcal{N}_i$, and $\varphi_j^* = 0$ for $j \notin \mathcal{N}_i$ belongs to the feasible set. For $W_i = 0$, we have $|\mathcal{N}_i \cap \mathcal{X}(W)| = k_i$:

$$\mathbb{P}[Z_i = 1|W] = 1-(1-\theta)^{k_i} \le k_i\theta$$
$$= \varphi_0^* + \sum_{k=1}^{n} \varphi_k^* W_k \tag{34}$$

For $W_i = 1$, it holds that $|\mathcal{N}_i \cap \mathcal{X}(W)| = k_i$:

$$\mathbb{P}[Z_i = 1|W] = 1-\gamma(1-\theta)^{k_i} \le 1-\gamma+k_i\theta$$
$$= \varphi_0^* + \sum_{k=1}^{n} \varphi_k^* W_k \tag{35}$$

Thus, φ^* is included in the feasible set.

$$\max_{\omega\mathcal{M}=p^T,\omega\ge 0} p_i(\tau+1)$$
$$= \min_{\varphi}\max_{\omega\ge 0} \omega\,(\mathcal{X}\mathcal{M}h_i - \mathcal{M}\varphi) + p^T\varphi$$
$$\le p^T\varphi^*$$
$$= (1-\gamma)p_i + \theta \sum_{j\in\mathcal{N}_i} p_j \tag{36}$$

Applying Lemma (2.4) to each node gives us:

$$p(\tau+1) \leq ((1-\gamma)A_{d_n} + \theta\mathcal{A})p(\tau) = \mathcal{M}p(\tau) \quad (37)$$

Furthermore, we can derive that the stationary distribution convergence time is $O(\log n)$ by modifying Theorem (2.1).

2.4 Reluctant Re-Engagement Dynamics in Digital Asset Participation

In this section, we will look at a *Reluctant Re-Engagement Model*. This model is designed to understand why people might hesitate to rejoin a digital asset system, like a cryptocurrency network, after they have stopped using it. Unlike simpler models where users might immediately come back after leaving, this model introduces a time delay. This suggest that if a user leaves the system (abandons), they are not likely to be convinced to return in the very next period, even if many of their connections are quite still active users. To give a more formal explanation to this, let's say $\eta_j(\tau)$ represents whether user j is participating at a specific time τ. The way these participation states change across the network is determined by the following probabilities:

$$P\left[\eta_j(\tau+1) = Z_j \mid \eta(\tau) = W\right] = \begin{cases} (1-\theta)^{k_j} & if \ \ (W_j, Z_j) = (N_a, N_a), |N_j \cap A(W)| = k_j \\ 1-(1-\theta)^{k_j} & if \ \ (W_j, Z_j) = (N_d, A_d), |N_j \cap A(W)| = k_j \\ \gamma & if \ \ (W_j, Z_j) = (A_d, N_a) \\ 1-\gamma & if \ \ (W_j, Z_j) = (A_d, A_d) \end{cases} \quad (38)$$

The model includes features where users don't usually rejoins after they stop participating, immediately. This reluctance to re-adopt right away makes the system less likely to quickly switch back and forth between using the asset and not using it. This leads to more a consistent long-term patterns, the estimated time for the network to reach a stable level of participation, which we can think of as the *time it takes to settle into a steady state*, is still within a limit of $O(\log N)$.

The main way we prove this settling time is similar to models where users rejoin immediately. The main change observed might is in how we are going to calculate the expected outcome under certain conditions:

$$\mathbb{P}[Z_j = \bar{1} \mid W] = \begin{cases} 1-(1-\theta)^{k_j} & \text{if} W_j = \bar{0}, \\ 1-\gamma & \text{if} W_j = \bar{1}. \end{cases} \quad (39)$$

A feasible vector $\omega^* = (\omega_0^*, \omega_1^*, \ldots, \omega_N^*)^\top$ may also be constructed with likely some components:

$$\omega_0^* = 0, \quad \omega_j^* = 1-\theta, \quad \omega_\ell^* = \gamma \text{ for } \ell \in \mathcal{N}_j, \quad \omega_\ell^* = 0 \text{ for } \ell \notin \mathcal{N}_j$$

The way the system changes over time can be represented by matrix called $\mathcal{M}$. This matrix is calculated by combining two main factors: $(1-\theta)$ multiplied by A_{d_n}, which represents the baseline adoption process, and γ multiplied by Γ, where Γ is a matrix showing the connections between every users in the network, this specific way of formulating the matrix guarantees that the system will eventually settle into a stable, long-term pattern of adoption.

III.RESULTS AND DISCUSSION

To test the model accuracy, a simulation is designed herein, over a variety of network topologies. Central to the model is the incorporation of peer driven and event driven adoption-abandonment probabilities, a mechanism that allows us to mimic the peer influence dynamics and event-driven behavior observed in real-world markets. The parameter settings of the network and their functional forms were carefully chosen to reflect plausible empirical patterns and theoretical justifications grounded in the behavior of digital asset (cryptocurrency and NFT) ecosystems (see Table 1).

Table 1: Justification of Parameter Choices in the Peer-Driven Digital Asset Adoption Model

Parameter	Value	Justification
n_{nodes}	≤ 10	Balance sample realism/computational cost
$m(BA)$	2	Realistic power-law networks (few hubs).

Parameter	Value	Justification
$p(ER)$	0.05	Sparse random networks (avg degree ~ 10).
$k, p(WS)$	4,0.1	Small-world with local clustering and few shortcuts.
$d(Regular)$	4	Uniform connectivity (e.g., ring networks).
Edge weights	[0.1,1]	Models varying influence strengths.

We now present simulation results on the *time to stationarity (mixing time)* of various network topologies, specifically: Scale-Free, Small-World, Erdős–Rényi Random, Regular, as well as Directed and Weighted networks. The goal is to examine how different structural configurations influence the rate at which a Markovian adoption–abandonment process converges to its stationary distribution. To reduce computational complexity, we restrict the network size to $n = 2^{10} = 1024$ nodes. This constraint enables the modeling of 2^{10} binary states representing individual agent choices (adopt or abandon), forming a state space of manageable size for simulation while preserving the essential dynamics of large-scale diffusion processes. We'll further explore how varying the event-driven sell-off probability (i.e., spontaneous abandonment) and peer-driven adoption probability (i.e., influence-based uptake) impacts the mixing time across these network structures. By doing so, we assess the sensitivity of mixing behavior to local decision-making mechanisms in different topological contexts.

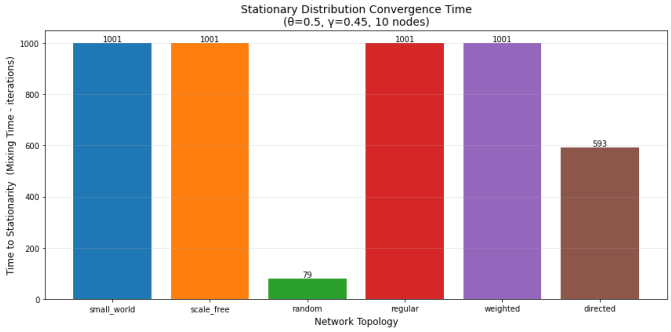

Figure 1: Mixing time across different network topologies with 45% sell off and 50% among 10 peers without re-engagement reluctance.

Figure (1) displays the mixing times for various network topologies (small world, scale-free, random, regular, weighted, and directed) in the Markov chain network (equation (4)) simulating digital asset abandonment (45% sell-off) and adoption (50% hold) among ten peers (not too far apart from % of sell-off). The small world, scale-free, regular, and weighted network topologies exhibit the longest times to stationarity (mixing time), all at 1001 steps. This indicates that these networks take a significantly longer time to reach a stable, "mixed" state where the influence of the initial distribution of digital assets has dissipated. The directed network has a slightly shorter mixing time at 593 steps, while the random network shows a considerably faster mixing time at only 79 steps. The implication of these mixing times for digital asset communities and markets is profound. For topologies with long mixing times (small world, scale-free, regular, weighted), information and behaviors (like sell-offs or holds) will propagate slowly through the community. This means that trends, price changes, or significant events in the digital asset market will take a long time to fully permeate and affect all participants. Such slow mixing could lead to delayed responses to market shifts, potentially creating opportunities for arbitrage for those with early information, or conversely, leaving some community members exposed to losses for longer periods as negative trends slowly diffuse. In contrast, the rapid mixing of the random network implies that information and behaviors spread very quickly and uniformly throughout the community. This would lead to more efficient markets where prices and community sentiment adjust rapidly to new information, reducing opportunities for exploitation and potentially leading to faster price discovery. The directed network, with its intermediate mixing time, suggests a moderate speed of information propagation,

likely influenced by the specific directional relationships between peers.

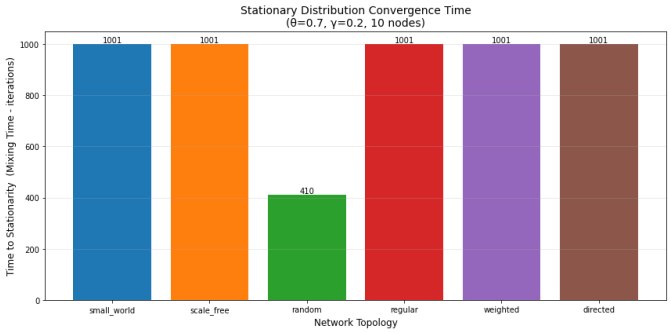

Figure 2: Mixing time across different network topologies with 20% sell off and 70% among 10 peers without re-engagement reluctance

Building upon the previous analysis, figure 2 illustrates the mixing times for the same network topologies, but under a different scenario: a 20% event-driven sell-off and a significantly higher 70% peer-driven hold of digital assets among ten peers. The stark difference between the hold and sell-off percentages is crucial here. Similar to the previous scenario, the small world, scale-free, regular, and weighted network topologies again exhibit the longest mixing times, all registering at 1001 steps. This reinforces the observation that these network structures inherently lead to protracted periods for the network to reach a stable equilibrium, irrespective of the specific sell-off/hold dynamics, provided the hold percentage is dominant. The directed network in this scenario also shows a very long mixing time of 1001 steps, which is a notable increase from its previous mixing time of 593 when the hold and sell-off percentages were closer. In contrast, the random network once again stands out with a significantly shorter mixing time, albeit longer than before, now at 410 steps. What this implies for digital asset communities and markets under this scenario, where holding behavior significantly outweighs selling, is that the large proportion of assets being held (70%) combined with the inherent characteristics of most network topologies (small world, scale-free, regular, weighted, and now also directed) leads to extremely slow information diffusion and behavioral shifts. Even with a high propensity to hold, the network's structural properties dictate how quickly the market reaches a consensus or stable state. This prolonged mixing time for most topologies suggests that, even when community sentiment is overwhelmingly geared towards holding, the market will still take a very long time to fully reflect this widespread sentiment or to effectively propagate any other significant market event. This could result in persistent price discrepancies or delayed market corrections, as information about the true supply and demand dynamics, or new fundamental information, takes a long time to permeate the entire community.

The random network, while still the fastest to mix, now takes 410 steps, considerably longer than its 79 steps in the previous scenario. This suggests that while randomness facilitates faster propagation, an extreme imbalance between sell-off and hold percentages can still slow down the overall mixing process even in highly interconnected random networks. In essence, with a strong hold sentiment, the market's natural tendency towards stability is significantly slowed down across almost all realistic network structures, potentially leading to prolonged periods of illiquidity or delayed price adjustments as information and behavioral shifts slowly ripple through the digital asset community.

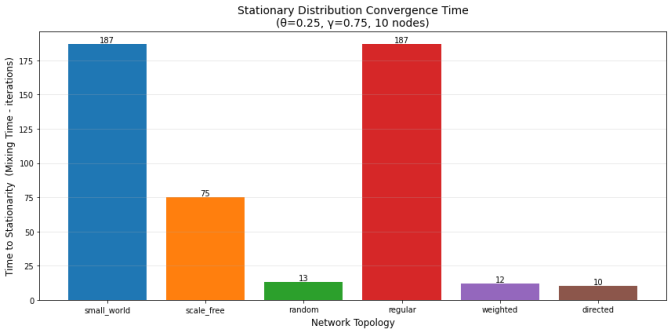

Figure 3: Mixing time across different network topologies with 75% sell off and 25% among 10 peers without re-engagement reluctance.

In figure 3, we consider a third scenario, focusing on a high event-driven sell-off (75%) and a low peer-

driven hold (25%) of digital assets among ten peers. The small world and regular network topologies once again exhibit identical mixing times, this time at 187 steps. These values are significantly lower than the 1001 steps observed in the previous two scenarios, indicating that when selling pressure is dominant, these network structures reach equilibrium much faster. The scale-free network also shows a considerably shorter mixing time at 75 units, a dramatic decrease from the previous 1001 steps. The weighted network and directed networks show the fastest mixing times at 12 and 10 units respectively, making them the most rapidly converging topologies under these conditions. The random network, while still relatively fast at 13 units, is no longer the absolute fastest, indicating that under extreme sell-off conditions, certain structured networks can become extremely efficient at disseminating information. Speaking further, it tells us that under a dominant sell-off environment is that information and behaviors related to selling will propagate much more rapidly across most network topologies compared to scenarios dominated by holding or balanced adoption/abandonment. The significantly reduced mixing times for small world, regular, and especially scale-free networks suggest that in a bear market or during a "panic selling" event, the market will reach a new equilibrium much quicker. This rapid mixing means that price discovery will be accelerated, and the impact of the sell-off will be felt across the entire community in a relatively short timeframe, leading to faster price depreciation and potentially quicker market capitulation. The weighted and directed networks, with their extremely low mixing times, would facilitate an almost immediate and widespread response to selling pressure, indicating that these structures are highly efficient at disseminating negative sentiment or information related to market downturns. The random network's continued quick mixing further supports the idea that less structured networks can quickly reach equilibrium, though in this case, it appears that very strong selling pressure can make even structured networks extremely efficient in disseminating negative sentiment. In essence, when sell-off behavior is dominant, the digital asset market, especially within small world, scale-free, regular, weighted, and directed network structures, will experience accelerated information flow and behavioral propagation. This would translate to quicker price adjustments and a more rapid establishment of a new, lower price equilibrium. Unlike the slow diffusion seen with strong holding behavior, a high sell-off percentage leads to a much more dynamic and rapidly responsive market environment, where collective actions quickly push the market towards a new state.

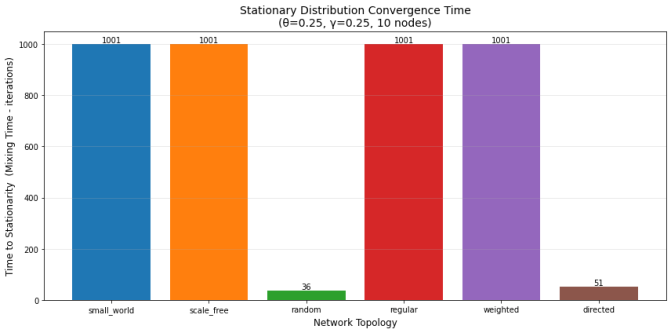

Figure 4 : Mixing time across different network topologies with 25% sell off and 25% among 10 peers without re-engagement reluctance.

It is evident from figure 4, that when the forces of selling and holding are in equilibrium (25% each, with an implied 50% "neutral" or other behavior), most structured networks (scale-free, small world, regular, weighted) still take an extremely long time to stabilize and reflect the true state of the market. This suggests that even with balanced forces, these complex networks inherently resist rapid information diffusion and behavioral convergence. For digital asset communities and markets, this implies that even minor events or shifts in sentiment could lead to prolonged periods of uncertainty and slow price discovery, as the network struggles to reach a new equilibrium. Trends, whether positive or negative, would propagate sluggishly, making it difficult for "faithfuls" (long-term holders or community members)

to quickly react or understand the true market consensus. The market would remain in a state of flux for extended periods, potentially leading to delayed reactions to news or fundamentals. Conversely, the random network, and to a lesser extent the directed network, would allow for quicker dissemination of information and behavioral shifts, leading to faster market adjustments.

As in figure 5, when there's a 50/50 split between sell-off and hold behaviors, the inherent slowness of mixing for scale-free, small world, and regular networks persists. This reinforces the idea that these common network structures are inherently resistant to rapid information flow and stabilization under conditions of balanced but high-activity (both selling and holding). For the digital asset market, this suggests that in periods of high indecision or balanced forces, these markets will struggle to find a stable equilibrium quickly. Prices and community sentiment would remain volatile and reactive over extended periods, making it challenging for both traders and the "faithful" to predict trends or understand the true underlying state of the market. The high mixing times imply that any shift in the market would take a substantial duration to be fully absorbed and reflected by the entire community. Interestingly, the random network's mixing time significantly increases from 36 to 123 steps when sell-off and hold percentages shift from 25% each to 50% each. This indicates that while random networks are generally faster to mix, higher activity levels (even if balanced) can still lead to slower overall convergence compared to extremely low activity. The weighted and directed networks, however, become relatively more efficient in this scenario, moving from 51 and 36 steps (for directed and random respectively, from Figure 4) to 63 and 59 steps. While their absolute values increase for the random network, their relative efficiency compared to the 1001-step networks becomes even more pronounced. This suggests that in highly active, undecided markets, the specific structure of weighted and directed relationships can facilitate somewhat quicker information propagation compared to other structured networks, offering a glimmer of faster equilibrium in certain scenarios.

Table 2: Summary of Mixing Times Across Different Network Topologies and Scenarios

Network Topology	Mixing Time (Steps)				
	45% Sell, 50% Hold	**20% Sell, 70% Hold**	**75% Sell, 25% Hold**	**25% Sell, 25% Hold**	**50% Sell, 50% Hold**
Small World	1001	1001	187	1001	1001
Scale-Free	1001	1001	75	1001	1001
Random	79	410	13	36	123
Regular	1001	1001	187	1001	1001
Weighted	1001	1001	12	1001	63
Directed	593	1001	10	51	59

For the markov chain with reluctant re-engagement of digital asset (see equation (38)), the mixing time stays uniform across different network topologies, it suggests that the constant, neighbor-independent abandonment rate is the dominant factor overriding the structural differences of the networks. This means the inherent topology of the community has little influence on how quickly the system reaches a stable state, likely because the consistent outflow from abandonment dictates the overall speed of change. For the community and market dynamics, this symbolizes that the "faithful" (long-term holders) are primarily affected by intrinsic, individual decisions to abandon assets, rather than by the influence of their peers or the structure of their social connections. The market, in turn, would experience a consistent, predictable decay or shift based on this underlying abandonment rate, with market dynamics being less responsive to peer-driven trends or network effects, and more driven by individual, event-triggered sell-offs. Based on our analysis of mixing times of the markov chain (4), for the sustainability of digital assets and increased

utility in Web3 projects, the ideal network type and associated mixing time would be one that balances efficient information dissemination with a degree of stability.

Given the goal of sustainability and increased utility, a random network appears to be the most advantageous to adapt. Its consistently lower mixing times across various scenarios, even in extreme sell-off or hold environments (though longer in high, balanced activity), indicate a faster propagation of information and quicker adaptation to new states. This means that positive news, utility updates, and community engagement would spread more efficiently, fostering adoption and loyalty. Conversely, negative events would also be processed and priced in more rapidly, leading to quicker market corrections and potentially less prolonged periods of uncertainty. Rapid mixing promotes market efficiency and allows for faster adaptation to changing conditions, which is crucial for the dynamic Web3 space. Below is a table summary of each network type's best fit in the Web3 and crypto/digital asset world:

Table 3: Network Topology Suitability in Web3 and Digital Asset Ecosystems

Network Topology	Best Suited For in Web3/Crypto/Digital Assets
Scale-Free	Ideal for platforms where a few highly connected "hubs" (e.g., influential community leaders, major exchanges, foundational protocols) are crucial for information dissemination and adoption. Excellent for viral growth and concentrated influence, but susceptible to single points of failure or manipulation if hubs are compromised.
Small-World	Great for fostering rapid communication and community building, as everyone is connected to everyone else by a short chain of acquaintances. Efficient for propagating trends, coordinating actions, and building strong, interconnected communities around a digital asset. Good for organic growth and decentralized governance.
Regular	Suited for highly structured, predictable, and permissioned environments, such as private blockchain consortiums or tightly controlled enterprise DLT applications where consistent and uniform information flow among well-defined peers is paramount. Less ideal for open, dynamic public crypto communities due to rigidity and slow mixing.
Random	Highly effective for achieving rapid and efficient information diffusion and price discovery in open and dynamic markets. Promotes resilience against targeted attacks (no central points of failure) and ensures quick response to market events, leading to more stable long-term asset value by quickly absorbing new information. Ideal for broad, decentralized adoption.
Directed	Useful for modeling specific relationships where influence or transactions flow in one direction, such as payment channels, influencer marketing campaigns, or governance structures where proposals flow from proponents to voters. Can represent information asymmetry or hierarchical decision-making within a community.
Weighted	Essential for representing varying strengths of relationships or transaction volumes between participants. Excellent for analyzing liquidity pools, staking relationships, or the economic impact of different actors. Allows for more nuanced modeling of influence and resource flow, providing a deeper understanding of economic stability and market depth.

3.1 Periodic Adoption and Event-Driven Abandonment

To model the fluctuating nature of asset adoption, we define the adoption rate as a periodic function that captures seasonal surges, such as those observed during events like Bitcoin halvings or tax deadlines. Specifically, the adoption rate $\theta(t)$ evolves as in equation (3), where $\theta_0 = 0.05$ serves as the baseline rate of organic, steady-state adoption, and $\Delta_\theta = 0.1$ introduces a fluctuation amplitude of 10%. This range is consistent with historical increases in adoption during major crypto events. The period $T = 365$ is chosen to align the oscillation with annual cycles, thereby embedding temporal seasonality into the model. In contrast, abandonment is modeled as a response to external shocks, such as security breaches or market crashes. The abandonment rate $\gamma(t)$ follows equation (2), with a maximum rate $\gamma_{\max} = 0.3$, reflecting intense but temporary panic-driven sell-offs. The steepness parameter $k_\gamma = 0.2$ ensures that this spike unfolds over approximately ten days, emulating the speed at which news spreads and behavioral contagion occurs. The shock is introduced at time $t_0 = 100$, mid-way through the simulation, to allow observation of the system's dynamics both before and after the disruptive event.

Table 4: Justification of Parameter Choices in the Peer-Driven Digital Asset Adoption Model

Parameter	Value	Justification
θ_0	0.5	Baseline organic adoption rate.
Δ_θ	0.1	Amplitude of seasonal adoption spikes (e.g., halvings).
T	365	Annual cycles (tax seasons, halvings).
$\gamma_{\max}$	0.3	Max abandonment during shocks (e.g., 30% sell-offs).
k_γ	0.02	Shock ramp-up speed ($\sim$ 10 days)
t_0	100	Mid-simulation shock to test resilience.
n_{nodes}	200	Balance realism/computational cost.
α	0.1	Peer influence aligned with empirical data.
$m(BA)$	2	Realistic power-law networks (few hubs).
$p(ER)$	0.05	Sparse random networks (avg degree $\sim$ 10).
$k, p(WS)$	4, 0.1	Small-world with local clustering and few shortcuts.
$d(Regular)$	4	Uniform connectivity (e.g., ring networks).
Edge weights	[0.1, 1]	Models varying influence strengths.

To explore how network topology shapes adoption and abandonment behavior, the simulation is done such that it generates networks consisting of $n_{\text{nodes}} = 200$ agents. This size is sufficient to yield emergent dynamics while keeping computational costs manageable. In *scale-free networks* constructed using the Barabási-Albert model, each new node forms $m = 2$ edges preferentially, promoting the emergence of hubs and a power-law degree distribution, traits common in influencer-driven markets like cryptocurrency ecosystems. In *Erdős-Rényi random graphs*, edges are added with probability $p = 0.05$, resulting in sparse and decentralized connectivity. This mimics trustless blockchain environments with minimal centralized control. The *Watts-Strogatz small-world networks* use $k = 4$ as the number of initial neighbors per node, and a rewiring probability $p = 0.1$. This setting strikes a balance between local clustering and global reach, closely resembling the structure of real-world social networks. For *regular networks*, a constant degree $d = 4$ is assigned to all nodes, offering a baseline scenario of uniform connectivity. In the case of *directed scale-free networks*, the edge formation is guided by parameters

$\alpha = 0.3$, $\beta = 0.4$, and $\gamma = 0.3$, which collectively control the preferential attachment and reciprocity. These settings are inspired by follower networks such as Twitter, where reciprocal relationships are common but not universal. Finally, to incorporate heterogeneous influence, *edge weights* are sampled uniformly from the interval [0.1,1.0], representing the varying strength of social ties, from casual followers to committed community members. The total simulation duration is set to $t_{\max} = 365$, corresponding to one year of daily updates. This will ensures that both seasonal adoption patterns and delayed shocks can be captured.

As earlier discussed in the previous sections, the dynamics of adoption and abandonment in digital asset networks can be understood through transition probabilities that govern node-level behaviors. Specifically, Equation (4) encapsulates the mechanisms of adoption (A_d) and abandonment (N_a) for each node. These transitions are influenced by several parameters: the peer-driven adoption probability θ, the abandonment probability γ, and the number of adopting neighbors denoted by k_j. A particularly notable feature of this model is its allowance for re-adoption nodes that have abandoned can freely return to the adoption state ($N_a \rightarrow A_d$).

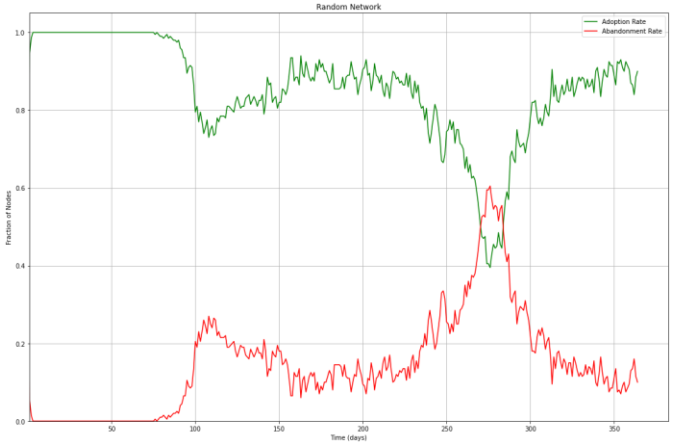

Figure 6: Periodic adoption (θ) and Event-driven abandonment (γ) rate over time across an Erdős-Rényi network ($p = 0.05$)

In figure 6, the dynamic interplay between periodic adoption (θ) and event-driven abandonment (γ) rates over a year in an Erdős-Rényi random network, is displayed. Initially, the adoption rate is very high, close to 1.0, while abandonment is negligible. Around day 75-80, there's a sharp decline in adoption and a corresponding rise in abandonment, indicating a significant sell-off or disengagement event. However, the network shows resilience, as adoption gradually recovers and abandonment subsides after this initial shock. A second, less severe dip in adoption and corresponding increase in abandonment occurs around day 250, but again, the network demonstrates a capacity for recovery. This suggests that in a random network, even with event-driven abandonment, the system can rebound and maintain a relatively high fraction of adopted nodes over time, indicating a robust and adaptable community.

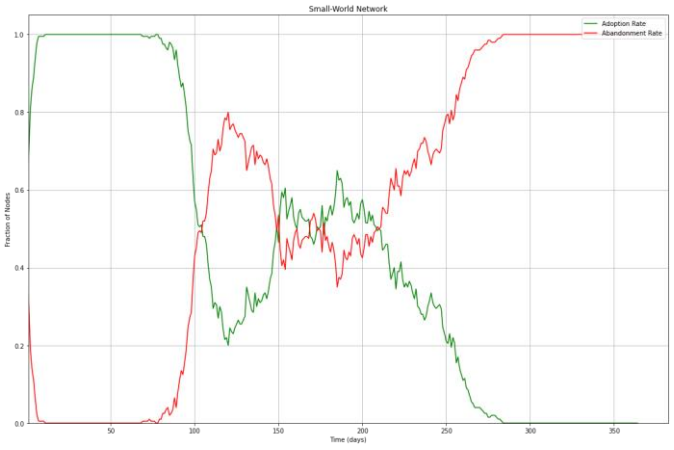

Figure 7: Periodic adoption (θ) and Event-driven abandonment (γ) rate over time across a Watts-Strogatz network ($k = 4, p = 0.1$)

The figure 7 shows the same dynamics but on a Watts-Strogatz small-world network. Here, the initial phase mirrors the Erdős-Rényi network with high adoption. However, the first abandonment event, occurring before day 100, is more pronounced and leads to a significant and sustained decline in adoption, with abandonment staying high for a prolonged period. While there are some fluctuations, the adoption rate struggles to recover to its initial levels. Towards the end of the year, the abandonment rate completely overtakes adoption, reaching 1.0 while adoption drops to 0. This indicates that in a Watts-

Strogatz network, the impact of event-driven abandonment, especially when coupled with periodic adoption, can lead to a more severe and potentially irreversible decline in the fraction of adopted nodes. The "small-world" nature, with its short path lengths and high clustering, might facilitate the rapid and widespread propagation of abandonment behavior, making the network more vulnerable to collapse if negative events are sufficiently strong and sustained. In essence, while the Erdős-Rényi network shows resilience and recovery, the Watts-Strogatz network appears more susceptible to prolonged negative trends leading to complete abandonment over the observed period.

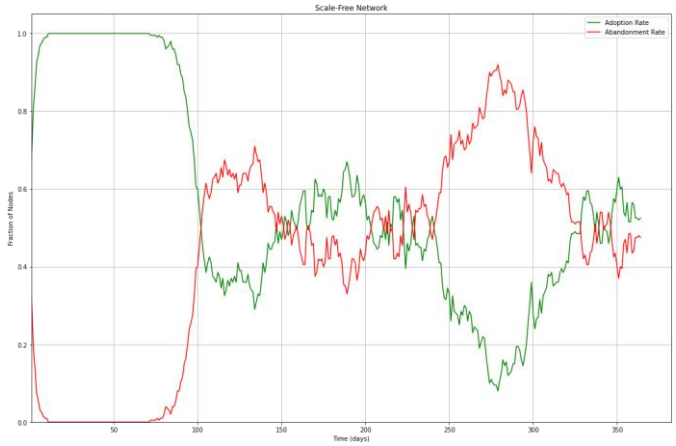

Figure 8: Periodic adoption (θ) and Event-driven abandonment (γ) rate over time across a Barabási-Albert network ($m = 2$)

In figure 8, adoption starts high and abandonment low. Just after day 50, a significant decline in adoption is mirrored by a surge in abandonment. However, unlike the Watts-Strogatz network's eventual collapse, the Barabási-Albert network shows a more volatile and oscillating pattern in the mid-period. Adoption and abandonment rates fluctuate, crossing paths multiple times between roughly day 150 and day 300, indicating a period of intense competition between forces of growth and decline. There's no clear dominance of either rate, suggesting that the network is in a state of dynamic equilibrium where the "hubs" in the scale-free network might be both driving adoption and, when events occur, contributing to abandonment. Towards the latter part of the year, after day 300, the adoption rate seems to stabilize at a moderately low level, with abandonment also fluctuating but not reaching its initial high peaks. This suggests that while scale-free networks can experience significant volatility and dramatic shifts in sentiment, they might eventually settle into a more dynamic, albeit lower, equilibrium where neither adoption nor abandonment fully dominates, reflecting the complex influence of highly connected nodes on information spread and behavioral changes.

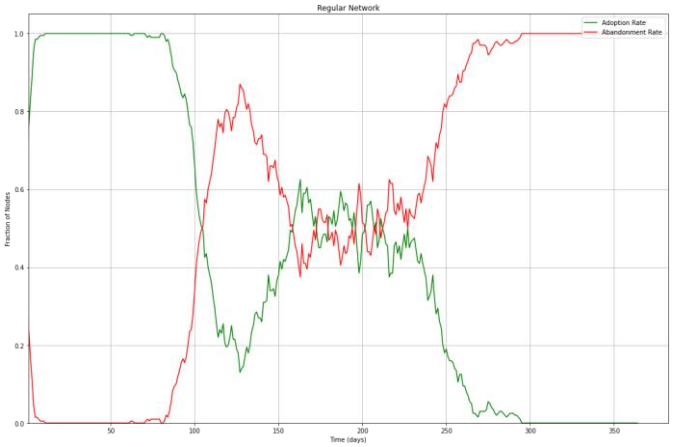

Figure 9: Periodic adoption (θ) and Event-driven abandonment (γ) rate over time across a Regular network (Ring with $k = 4$)

Similar to the other network types, in figure 9 adoption starts high while abandonment is low. Around day 65, a rapid decline in adoption is met with a sharp increase in abandonment, mirroring the initial pattern seen across all analyzed network types. The unique characteristic of the regular network, however, is observed in the subsequent phase. After the initial crash, there's a period of significant volatility and oscillation where adoption and abandonment rates frequently cross and fluctuate, often appearing to mirror each other. This dynamic equilibrium persists for an extended period, roughly from day 150 to day 300, without either force decisively dominating. Towards the end of the year, a second, more pronounced surge in abandonment occurs, pushing the adoption rate down to near zero by day 365, indicating a complete shift in sentiment

and a full abandonment of the asset within this network structure. This suggests that while regular networks might initially resist a complete collapse by maintaining a prolonged period of oscillation, they are ultimately susceptible to widespread abandonment under sustained pressure, particularly if the initial events trigger a significant outflow that the rigid structure cannot effectively counter.

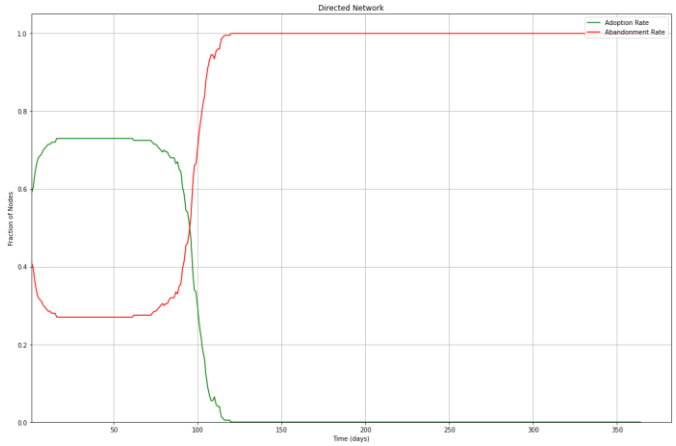

Figure 10: Periodic adoption (θ) and Event-driven abandonment (γ) rate over time across a Directed network

At the onset, figure 10, shows adoption rate is high, hovering around 0.6 to 0.7, while the abandonment rate is very low, near 0.3. Around day 100, a dramatic shift occurs: the adoption rate sharply declines, plummeting to near zero by approximately day 150. Simultaneously, the abandonment rate experiences a rapid surge, reaching its peak at 1.0 around day 150 and remaining at that maximum level for the rest of the year. This distinct pattern in a directed network suggests that initial adoption is present but susceptible to a sudden and complete reversal. The directional links might facilitate a rapid and unidirectional flow of negative sentiment or information during an abandonment event, leading to a swift and total loss of adoption from which the network cannot recover. This highlights a vulnerability in directed networks where the influence structure can quickly lead to widespread abandonment once a critical threshold is crossed, without any subsequent recovery in adoption.

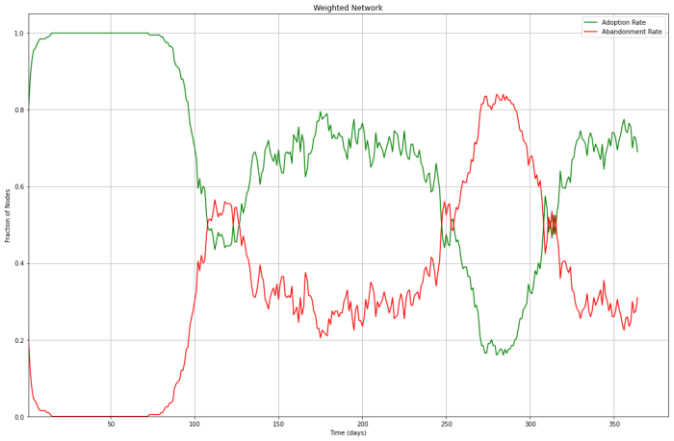

Figure 11: Periodic adoption (θ) and Event-driven abandonment (γ) rate over time across a Weighted network

Lastly, the initial pattern of figure 11, mirrors the other network types: high adoption and negligible abandonment. Before day 100, a sharp decline in adoption is observed, met by a corresponding surge in abandonment. However, what distinguishes the weighted network is the subsequent long period of volatile oscillation. From roughly day 100 to day 300, both adoption and abandonment rates fluctuate significantly, crossing over multiple times. The weighted connections likely mean that stronger ties between nodes have a more substantial impact on the propagation of sentiment, leading to more pronounced swings as adoption and abandonment forces battle for dominance. This creates a highly dynamic and unpredictable environment where the prevailing trend is not stable. Towards the end of the year, a second, more severe decline in adoption occurs, again accompanied by a rise in abandonment, although it doesn't reach 1.0 like in the Directed or Watts-Strogatz cases. This suggests that while weighted networks can experience prolonged periods of instability and struggle to find a clear equilibrium under these dynamics, the varying strengths of connections might prevent a complete and sustained collapse of adoption, instead fostering continuous, albeit volatile, interaction between adopting and abandoning behaviors.

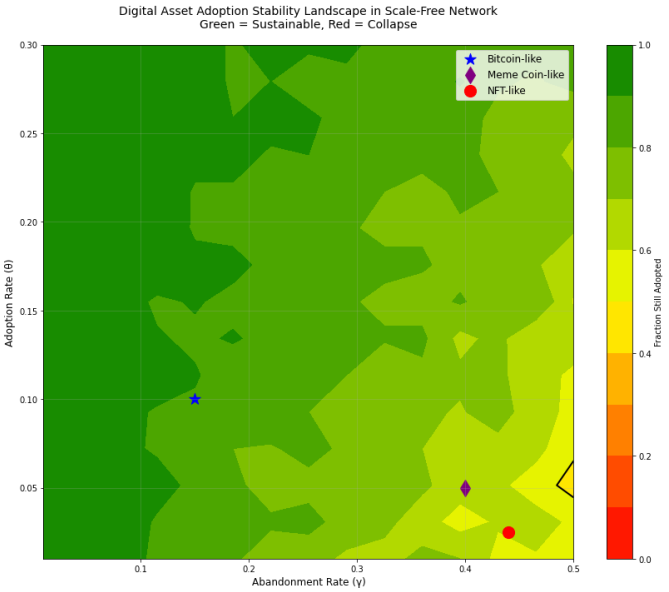

Figure 12: Phase diagram of adoption stability landscape in Scale-Free Network

The phase diagram in figure 12 −17, illustrates the adoption stability landscape in the various network topologies, where the intensity of spread is color-coded from green (low) to red (high). The x-axis represents the abandonment rate, while the y-axis denotes adoption levels. The landscape exhibits regions of varying stability, with higher adoption and lower abandonment rates typically associated with more stable, sustainable adoption (green), whereas higher abandonment rates and lower adoption lead to instability (red).

The blue star, representing Bitcoin-like assets, is positioned in a region of high adoption and relatively low abandonment, indicating robust and stable adoption. This aligns with Bitcoin's dominant role in the cryptocurrency ecosystem, characterized by widespread acceptance and resilience to abandonment. The red circle, marking NFT-like assets, appears in a less stable region with moderate adoption but higher abandonment, reflecting their niche and often speculative nature. The purple diamond, denoting Meme coin-like assets, lies in an area of lower adoption and higher abandonment, highlighting their volatility and dependence on short-term trends.

Bitcoin's dominance in these landscapes is evident from its placement in the most stable and sustainable region, underscoring its entrenched position as a foundational asset with enduring adoption. In contrast, NFT-like and Meme coin-like assets occupy more precarious zones, reflecting their susceptibility to rapid shifts in interest and higher abandonment rates. The vertical scale for "fraction still adopted" further reinforces Bitcoin's superior retention and staying power compared to the other asset types.

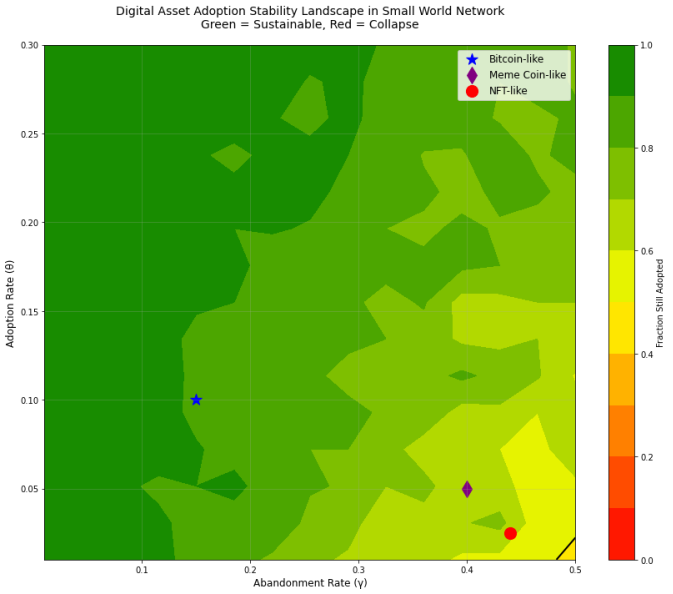

Figure 13: Phase diagram of adoption stability landscape in Small-World Network

In all our analysis has illuminate behavioral regimens, for Directed and Weighted networks, their behavior often reflects subtle yet powerful influences on adoption and abandonment. When $\theta \gg \gamma$, indicating a strong bias towards adoption, directed networks, particularly those with high in-degree variance, can exhibit a "winner-takes-all" dynamic, where the digital asset rapidly achieves and sustains high adoption, similar to the initial high adoption observed in their respective individual analyses. Conversely, when $\theta \ll \gamma$, a strong out-degree correlation in directed networks can dramatically accelerate abandonment cascades, quickly driving adoption to near zero, as seen in the figure 10, where adoption completely collapses. In weighted networks, the ratio of strong to weak ties plays a pivotal role. A low ratio of strong ties might lead to abandonment patterns that decay exponentially, signifying a more contained and

predictable decline. However, a high ratio of strong ties can produce power-law decay in abandonment, suggesting that major shocks could disproportionately impact the network, leading to widespread and persistent disengagement. When $\theta \approx \gamma$, both directed and weighted networks can exhibit prolonged periods of oscillation, as observed in figure 11, where the tug-of-war between adoption and abandonment creates a volatile and uncertain landscape.

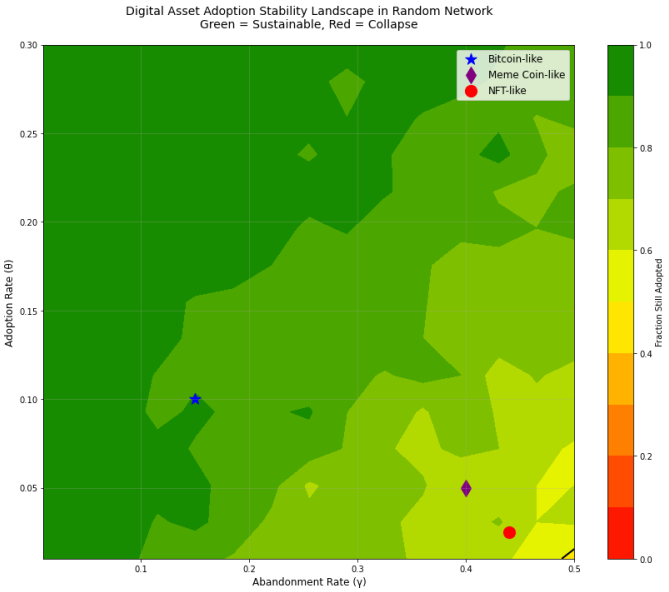

Figure 14: Phase diagram of adoption stability landscape in Random Network

Regular networks, characterized by their uniform connections, tend to behave distinctly. In a high-adoption environment ($\theta \gg \gamma$), regular networks can achieve and maintain strong adoption. However, when $\theta \approx \gamma$, these networks display a protracted period of volatile oscillation between adoption and abandonment, as evidenced in figure 14. This suggests a struggle to achieve stability, where the rigid structure doesn't easily facilitate a decisive shift. Ultimately, when $\theta \ll \gamma$, regular networks are highly susceptible to eventual widespread abandonment, with adoption plummeting to near zero after prolonged instability, reflecting a lack of inherent resilience to strong negative pressures.

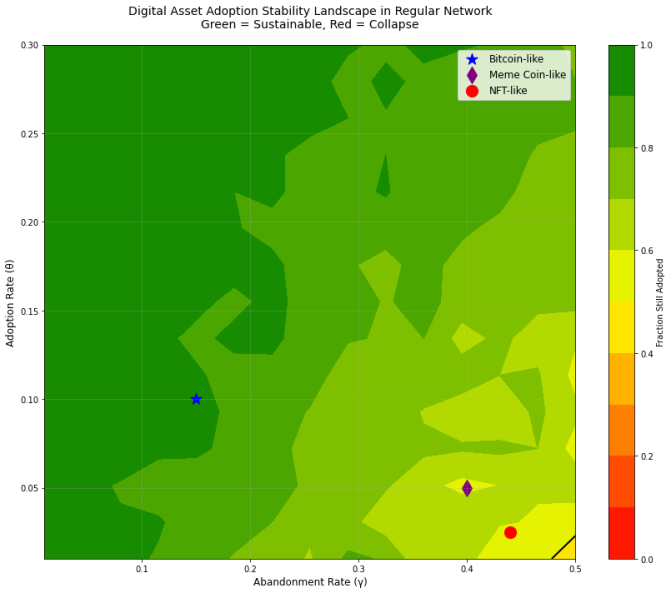

Figure 15: Phase diagram of adoption stability landscape in Regular Network

Random networks, due to their inherent structural disorder, demonstrate a more consistent and often faster response to changes in adoption and abandonment rates. In the sustainable adoption regime ($\theta \gg \gamma$), random networks rapidly achieve high adoption, albeit perhaps not reaching the initial peak levels seen in some structured networks, as suggested by figure 1, where adoption recovers but not fully. When $\theta \approx \gamma$, the system can enter a metastable state where the network topology significantly influences survival, reminiscent of meme coins' fragile dynamics. However, random networks generally exhibit quicker mixing times, enabling faster resolution of such states compared to more structured networks. In the rapid abandonment regime ($\theta \ll \gamma$), random networks facilitate quick and relatively uniform disengagement, leading to widespread abandonment, as shown by their lower mixing times in various sell-off scenarios.

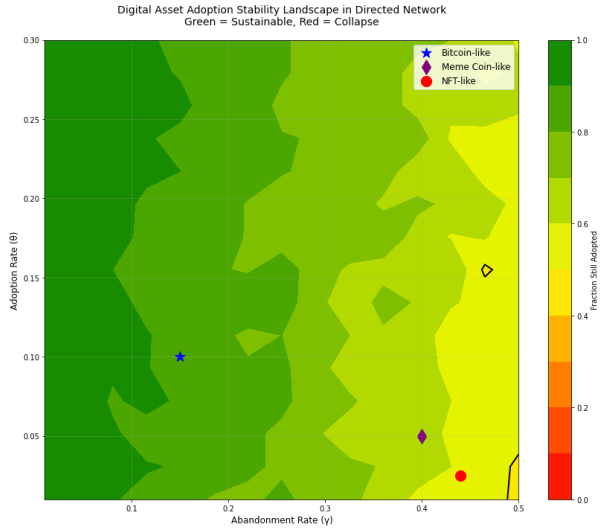

Figure 16: Phase diagram of adoption stability landscape in Directed Network

The Small-World network topology presents a paradox. While its shortcuts are highly effective at expediting initial adoption and spreading positive sentiment, as seen in the early high adoption in figure 2, they simultaneously introduce a wide variance in abandonment. This "small-world paradox" implies that while some nodes might abandon orders of magnitude later than others due to the network's shortcuts, a critical collapse ($\theta \approx \gamma$) can lead to a rapid and almost complete shift towards abandonment, as the negative sentiment quickly propagates through these very same shortcuts, causing the system to reach near-zero adoption in the long run.

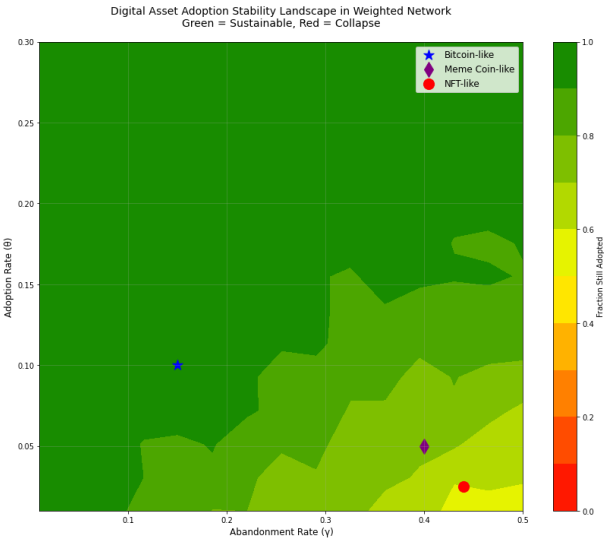

Figure 17: Phase diagram of adoption stability landscape in Weighted Network

Finally, Scale-Free networks, with their hub-and-spoke architecture, demonstrate unique characteristics. In the sustainable adoption regime ($\theta \gg \gamma$), adoption spreads rapidly and is retained, with the network stabilizing at over 80% adoption, mirroring the behavior of established cryptocurrencies like Bitcoin. A mere 5% of nodes (the hubs) in scale-free networks can dictate 95% of adoption and abandonment timelines, highlighting their immense influence. This means that a relatively small number of highly connected individuals or entities significantly control the market's direction. Conversely, removing just the top 1% of these influential nodes can decuple (10x) the abandonment for the entire network when $\theta \ll \gamma$, showcasing extreme vulnerability to targeted shocks. When $\theta \approx \gamma$, the system enters a highly volatile metastable state, as depicted in figure 8, where the struggle between adoption and abandonment can lead to prolonged oscillations due to the concentrated influence of the hubs.

IV. CONCLUSION

Our extensive analysis of digital asset adoption and abandonment dynamics within Markov chain networks has provided significant insights into the intricate relationship between network topology and market behavior. The investigation into mixing times consistently demonstrated that highly structured networks such as scale-free, small-world, and regular networks generally exhibit prolonged periods to reach a stationary state, suggesting slower information diffusion and delayed market equilibrium. Conversely, random networks, and under specific conditions, weighted and directed networks, often displayed considerably faster mixing, indicating more efficient information propagation and quicker responses to shifts in adoption and abandonment rates. The inclusion of reluctant re-engagement further modulated these dynamics, emphasizing the persistence of abandonment in certain scenarios.

The simulation dynamics across various network types painted a nuanced picture: while some networks like the Watts-Strogatz small-world can experience rapid and near-total abandonment under specific conditions, others like the Barabási-Albert scale-free networks may enter prolonged periods of volatility and oscillation before potentially stabilizing at a lower equilibrium. The phase diagrams powerfully illustrated that sustainable adoption is typically achieved when adoption rates significantly outpace abandonment, a regime where Bitcoin-like assets consistently reside. Conversely, a balance between adoption and abandonment can lead to critical, topology-dependent metastable states, and a dominance of abandonment invariably results in rapid, widespread disengagement. This analysis strongly suggests that for the long-term sustainability and utility of digital assets in the Web3 space, adapting to network structures that facilitate faster mixing, such as a random network, would be highly beneficial, enabling quicker assimilation of positive developments and more rapid recovery from adverse events. The inherent properties of each network type dictate how resilient a digital asset community will be to external shocks and how efficiently information and sentiment will propagate, ultimately shaping the asset's market value and utility.

4.1 Further Direction

Future research should aim to validate these theoretical models with real-world digital asset market data, incorporating empirical evidence of peer-to-peer interactions and event-driven abandonment triggers. Exploring more complex, dynamic network evolution models, where the network structure itself changes over time in response to adoption and abandonment, would provide richer insights. Additionally, investigating the impact of multi-asset interactions, regulatory interventions, and the role of sentiment analysis derived from social media on these dynamics could offer a more holistic understanding. Developing predictive frameworks that leverage network metrics to forecast adoption trends and identify potential vulnerabilities within digital asset ecosystems would also be a valuable extension of this work.

REFERENCES

[1]. Ahn, H. and Hassibi, B. (2014). On the mixing time of the sis markov chain model for epidemic spread. 53rd IEEE Conference on Decision and Control, pages 6221–6227.

[2]. Allassak, N., Trichni, S., and Omary, F. (2024). A comprehensive cryptocurrency approach based on a customized peer-to-peer network. Proceedings of the 7th International Conference on Networking, Intelligent Systems and Security.

[3]. Angorani, S. (2024). Global dynamics of cryptocurrency adoption: An empirical exploration of fintech's influence on the evolution of digital currencies. Indonesian Journal of Economics, Business, Accounting, and Management (IJEBAM).

[4]. Blumberg, O., Morris, B., and Senda, A. (2024). Mixing time of the torus shuffle.

[5]. Boralkar, M., Khan, A., and Salunkhe, H. A. (2024). Emprical study of crypto currency and its adoption among indians. 2024 International Conference on Trends in Quantum Computing and Emerging Business Technologies, pages 1–5.

[6]. Chakrabarti, D., Wang, Y., Wang, C., Leskovec, J., and Faloutsos, C. (2008). Epidemic thresholds in real networks. ACM Transactions on Information and System Security (TISSEC), 10(4).

[7]. Cipriani, A. and Salvi, M. (2021). Scale-free percolation mixing time. Stochastic Processes and their Applications.

[8]. Ebizie, P. I., Nkamnebe, A., and Ojiaku, O. C. (2022). Factors influencing cryptocurrency adoption among nigerian university fintech

entrepreneurs: An utaut perspective. British Journal of Marketing Studies, 10(3):25–37.

[9]. ElBahrawy, A., Alessandretti, L., Kandler, A., Pastor-Satorras, R., and Baronchelli, A. (2017). Evolutionary dynamics of the cryptocurrency market. Royal Society Open Science, 4.

[10]. Emunefe, F. G. and Ugbene, I. J. (2024). Jukes-cantor correction for phylogenetic tree reconstruction. bioRxiv.

[11]. Fang, X., Hu, P. J., Li, Z., and Tsai, W. (2012). Predicting adoption probabilities in social networks. Technology.

[12]. Gao, P. and Greenhill, C. S. (2020). Mixing time of the switch markov chain and stable degree sequences. Discret. Appl. Math., 291:143–162.

[13]. Hafid, A., Ebrahim, M., Alfatemi, A., Rahouti, M., and Oliveira, D. (2024). Cryptocurrency price forecasting using xgboost regressor and technical indicators. 2024 IEEE International Performance, Computing, and Communications Conference (IPCCC), pages 1–6.

[14]. John, D. L., Binnewies, S., and Stantic, B. (2024). Cryptocurrency price prediction algorithms: A survey and future directions. Forecasting.

[15]. Kajol, K., Devarakonda, S., Singh, R., and Baker, H. K. (2025). Drivers influencing the adoption of cryptocurrency: a social network analysis approach. Financial Innovation.

[16]. Kayoh, C. O. and Ugbene, I. J. (2023). Towards mechanism-based interventions for auxin signaling: Application of algebraic edge control to a boolean network model. International Journal of Mathematical Analysis and Modelling, 6(2).

[17]. Kimmel, N., Kong, L., and Wang, M. (2024). Modeling the dynamics of user adoption and abandonment in online social networks. Mathematical Methods in the Applied Sciences, 48:1853 – 1868.

[18]. Kimmerl, J. (2020). Understanding users' perception on the adoption of stablecoins - the libra case. In The Pacific Asia Conference on Information Systems 2020 (PACIS 2020), page 187.

[19]. Kong, L. (2024). Modelling the dynamics of product adoption and abandonment. Proceedings of the Royal Society A, 480:20240034.

[20]. Kremer, G. E. O., Chiu, M., and Kim, T.-H. (2013). Perceived feature utility-based product family design: a mobile phone case study. Journal of Intelligent Manufacturing, 24:935–949.

[21]. Li, C.-T., Lin, Y.-J., and Yeh, M.-Y. (2018). Forecasting participants of information diffusion on social networks with its applications. Inf. Sci., 422:432–446.

[22]. Nuwan, A., Bandara, H., Ranasinghe, D., Heenkenda, S., B.W.R, D., Perera, A., and Bulankulama, S. (2025). Does financial stability moderate the nexus between the factors and cryptocurrency adoption as a mode of payment in sme sector in sri lanka. International Journal of Research and Innovation in Social Science.

[23]. Osanakpa, R. O. and Ugbene, I. J. (2025). Modeling meiotic rearrangements: Using dynamic programming to elucidate the role of dna alignments in ciliate reproduction. FUPRE Journal of Scientific and Industrial Research, 9(1):01–13.

[24]. Pesch, R., Endres, H., and Bouncken, R. B. (2021). Digital product innovation management: Balancing stability and fluidity through formalization. Journal of Product Innovation Management.

[25]. Ramkumar, A. and Soleimanifar, M. (2024). Mixing time of quantum gibbs sampling for random sparse hamiltonians. ArXiv, abs/2411.04454.

[26]. Rodpangtiam, A., Boonchutima, S., and Mazahir, I. (2024). Perception of social media users regarding cryptocurrency investment adoption: a case of social media platform – reddit. Cogent Business & Management, 11.

[27]. Ruhi, N. A. and Hassibi, B. (2015). Sirs epidemics on complex networks: Concurrence of exact markov chain and approximated models. 2015 54th IEEE Conference on Decision and Control (CDC), pages 2919–2926.

[28]. Saiedi, E., Brostrom, A., and Ruiz, F. (2021). Global drivers of cryptocurrency infrastructure adoption. Small Business Economics, 57(2):353–406.

[29]. Sergio, I. and Wedemeier, J. (2025). Global surge: exploring cryptocurrency adoption with evidence from spatial models. Financial Innovation.

[30]. Shahzad, M. F., Xu, S., Lim, W. M., Hasnain, M. F., and Nusrat, S. (2024). Cryptocurrency awareness, acceptance, and adoption: the role of trust as a cornerstone. Humanities and Social Sciences Communications, 11:1–14.

[31]. Ugbene, I. J. and Agwemuria, R. O. (2024). Identifying control targets for regulating mild cognitive impairment using reduced computational models of a life kinetic network. FUPRE Journal of Scientific and Industrial Research, 8(1):23–38.

[32]. Ugbene, I. J. and Ajuremisan, I. S. (2025). State space analysis of diphtheria pathogenesis using semi-tensor products and permutation methods. Network Biology, 15(4):123–149.

[33]. Ugbene, I. J., Bakare, G. N., and Ibrahim, G. R. (2019). Conjugacy classes of the order-preserving and order-decreasing partial one-to-one transformation semigroups. FUTMINA.

[34]. Ugbene, I. J. and Makanjuola, S. O. (2012). On the number of conjugacy classes in the injective order-preserving transformation semigroup. Icastor Journal of Mathematical Sciences, 6(1).

[35]. Ugbene, I. J., Makanjuola, S. O., and Eze, E. O. (2013). On the number of conjugacy classes in the injective order-decreasing transformation semigroup. Image, 1.

[36]. Ugbene, I. J. and Mbah, M. A. (2015). On the combinatorial properties of nilpotent and idempotent conjugacy classes of the injective order-decreasing transformation semigroup. FULafia Journal of Science and Technology, 1(1):91–94.

[37]. Ugbene, I. J., Ogundele, S. O., and Ndubuisi, R. U. (2022). Digraph of the full transformation semigroup. Journal of Discrete Mathematical Sciences and Cryptography, 25(8):2457–2465.

[38]. Ugbene, I. J. and Utoyo, T. O. (2024a). Determining synchronously updated fixed points and attractors in a prototype boolean gene regulation model of diphtheria pathogenesis. Open Journal of Mathematical Sciences, 8:167–184.

[39]. Ugbene, J. I. and Utoyo, T. O. (2024b). Switching stomatal aperture dynamics through computationally algebraic node control. FUPRE Journal of Scientific and Industrial Research, 8(1):136–144.